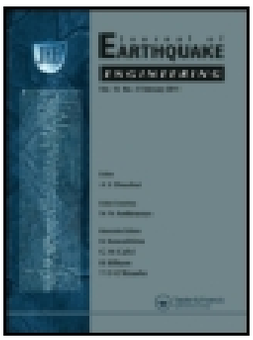

Journal of Earthquake Engineering

ISSN: 1363-2469 (Print) 1559-808X (Online) Journal homepage: http://www.tandfonline.com/loi/ueqe20

Modelling the seismic response of modern URM buildings retrofitted by adding RC walls

Alessandro Paparo & Katrin Beyer

To cite this article: Alessandro Paparo & Katrin Beyer (2015): Modelling the seismic response of modern URM buildings retrofitted by adding RC walls, Journal of Earthquake Engineering, DOI: 10.1080/13632469.2015.1091798

To link to this article: http://dx.doi.org/10.1080/13632469.2015.1091798

Accepted author version posted online: 24 Nov 2015.

Modelling the seismic response of modern URM buildings retrofitted by adding RC walls

Alessandro Paparo [a)], Katrin Beyer [b)*]

[a)] Earthquake Engineering and Structural Dynamics Laboratory (EESD), School of Architecture, Civil and Environmental Engineering (ENAC), École Polytechnique Fédérale de Lausanne (EPFL), Switzerland. EPFL ENAC IIC EESD, GC B2 515, Station 18, CH – 1015 Lausanne Tel: +41 21 6936321 alessandro.paparo@epfl.ch

[b)] Earthquake Engineering and Structural Dynamics Laboratory (EESD), School of Architecture, Civil and Environmental Engineering (ENAC), École Polytechnique Fédérale de Lausanne (EPFL), Switzerland. EPFL ENAC IIC EESD, GC B2 504, Station 18, CH – 1015 Lausanne Tel: +41 21 6936234 Tel: +41 21 6935706 katrin.beyer@epfl.ch

*** Corresponding author**

Abstract

Modern unreinforced masonry buildings with reinforced concrete slabs are often retrofitted by inserting reinforced concrete walls. The main advantages of this technique are the increase in strength and displacement capacity with respect to masonry structures. The paper presents two modelling approaches for evaluating such structures: a shell-element model and a macro-element one. The objective is to formulate practical recommendations for setting up a macro-element model using as input the geometry of the structure and results from standard material tests. Structural configurations of masonry buildings, in which the insertion of reinforced concrete walls is an efficient retrofit technique, are also investigated.

Keywords Seismic behaviour Modern mixed masonry and reinforced concrete wall structures Non-linear analyses Shell-element model Macro-element model Equivalent frame

1. Introduction

In recent years, the seismic hazard in several countries of Europe was re-evaluated, leading, in particular for countries of low to moderate seismicity to an increase of the seismic design spectra. As a result, many modern residential unreinforced masonry (URM) buildings no longer fulfil the seismic design check for the new spectra and have to be retrofitted. Adding RC walls to the existing structure or replacing selected URM walls with RC ones can be an effective retrofit strategy if RC slabs allow a redistribution of the forces. This retrofit approach might not only increase the strength but also modify the global deformed shape of the structure, leading to an increase in the system's displacement capacity. For new constructions, it is pertinent to conceive similar structures directly as mixed RC-URM systems because they show an improved seismic behaviour when compared to buildings with URM walls only. In addition, when compared to buildings with RC walls only, such mixed structures have better thermal and insulation properties at a lower construction cost.

Mixed RC-URM construction varies significantly from region to region [Magenes, 2006; Cattari and Lagomarsino, 2013]. In this paper, the examination is limited to the most common building configurations of modern mixed RC-URM systems built in Switzerland. Such configurations are characterised by the following features:

i) The RC-URM systems are modern buildings of three to five storeys with masses evenly distributed over the height. Both masonry and concrete walls are continuous over the height and

connected at each floor by 20 to 30 cm thick RC slabs which provide an efficient rigid diaphragm.

ii) The length of the RC walls varies between 2 and 5 m and their aspect ratio is between 1.5 and 3. The RC walls are 20 to 30 cm thick and designed according to modern codes to develop a stable flexural behaviour with displacement capacities larger than those of URM walls. The mean concrete cylinder compressive strength at 28 days is between 20 and 50 MPa and the reinforcement bars have mean yield strengths between 500 and 600 MPa. The total longitudinal reinforcement ratio of the RC walls varies between 0.2% and 4.0% [EN 1992-1, 2004]. In the RC slabs the longitudinal reinforcement ratio varies between 0.13% and 4.0% [EN 1992-1, 2004].

iii) The URM walls have typically lengths up to 7 m and aspect ratios between 0.5 and 3. The URM walls, which always outnumber the RC ones, are built with hollow clay 20 to 30 cm thick bricks in combination with standard cement mortar. URM walls are characterised by mean masonry compressive strengths (f_{cM}) between 4 and 8 MPa and axial stress ratios (σ_0/f_{cM}) between 0.05 and 0.25. Since in such structures the URM walls are connected by RC slabs which introduce an important framing effect [Lang, 2002], the URM walls generally exhibit a dominant shear behaviour.

Despite the popularity of this construction and retrofitting technique, very little research has been carried out [Magenes, 2006] and there are several open issues to be addressed:

i) Response of mixed RC-URM wall structures: Vertical and horizontal forces are resisted by the combined contribution of the existing URM walls and the new RC walls. Hence the retrofitted

structure will behave differently from the uncoupled systems since each type of wall results in a different displaced shape when subjected to horizontal forces (Fig. 1).

ii) Lack of experimental data: There are only few experimental tests on mixed RC-URM structural buildings. Tomaževič *et al.* [1990] conducted a shake table test on a URM wall building with one RC column. However, the latter had no influence on the behaviour of the structure under lateral loads since the URM walls were considerably stiffer. Jurukovsky *et al.* [1992] conducted shake table tests of 1/3-scale models. They investigated several strengthening techniques for a mixed structure composed of URM walls and one RC frame at the ground floor. In one case they added a central RC core wall to the URM building and they tested this retrofitted solution up to the near collapse limit state, but the presence of the RC frame at the ground floor added a vertical irregularity. Hence, none of the experimental studies addressed the seismic behaviour of mixed structures where RC and URM walls are regular and continuous over the height.

iii) Numerical modelling: Numerical results on RC-URM wall structures are sensitive to mechanical and geometrical assumptions [Casoli, 2007; Paparo and Beyer, 2012] but models could not be validated as experimental results of such mixed structures were missing. For these buildings, the parameters which most influence the distribution of reaction forces among the walls are those defining the strength and stiffness of the elements.

iv) Scarce numerical investigations: Recently non-linear numerical investigations [Cattari and Lagomarsino, 2013] studied the interaction of RC and URM walls. They simulated the response of buildings where the RC walls were not capacity-designed and failed before the URM walls.

The study presented herein targets structures where the RC members are designed to fail for larger displacement demands than the URM walls.

In order to address the aforementioned issues, a research programme was initiated at EPFL with the objective to understand better the seismic behaviour of mixed RC-URM wall structures. Both experimental (Fig. 2 and 3) and numerical investigations were carried out. The objective of this paper is to provide some indications for the modelling and analysis of structures with both RC and URM walls. Two modelling approaches will be investigated: a shell-element model and a macro-element approach; the latter is commonly used in engineering practice for analysing such structures. Sec. 2 will present the main characteristics of the seismic behaviour of mixed RC-URM wall structures and will outline advantages and drawbacks of coupling URM walls with RC walls. In Sec. 3 the two modelling approaches will be presented and validated against experimental results. The paper concludes with the discussion of four case studies (Sec. 4), outlining for which structural configurations of URM buildings adding RC walls can be an efficient retrofit measure.

2. Seismic behaviour of interacting URM and RC walls

Retrofitting a modern URM building by replacing some URM walls with RC ones does not only increase the strength of the structure, but can also improve the system's displacement capacity. The section describes qualitatively the interaction of URM and RC walls connected by RC slabs

when subjected to lateral forces (Sec. 2.1) and outlines the resulting advantages and disadvantages of this retrofit technique (Sec. 2.2).

2.1. Deformation pattern of mixed RC-URM wall structures subjected to lateral loading

URM walls have a dominant flexural or shear response depending on several parameters such as the axial load ratio, the pier geometry and the coupling moment introduced by RC slabs or masonry spandrels. RC walls are designed to have a dominant flexural behaviour and a displacement capacity larger than that of URM walls. The RC slabs are assumed to provide a rigid diaphragm action, allowing an effective force redistribution between walls of one plane.

Under lateral loading, uncoupled URM walls which deform primarily in shear lead to larger inter-storey drifts at the bottom storeys (Fig. 1a). Single slender RC walls display instead primarily flexural deformations, with larger inter-storey drifts at top storeys (Fig. 1b). At the height of the RC slabs, URM and RC walls need to displace by the same amount because of the rigid diaphragm action provided by the RC slabs. Hence, the deformed shape of mixed RC-URM wall structures lies in between that of buildings with RC and URM walls alone (Fig. 1c). As a consequence, for such mixed structures the damage in the URM walls is not concentrated in the first storey—as for URM buildings—but it also spreads to the storeys above. This behaviour was noted in quasi-static and dynamic tests on mixed RC-URM wall structures (Fig. 2 and 3) and also Jurukovsky *et al*. [1992] observed that the presence of the pin-based RC wall "distributed the failure mechanism all over the structure".

Mixed RC-URM wall structures present similarities to dual RC frame-wall buildings. Slender wall elements, which display mainly flexural deformations, are coupled to frames, which globally deform—as do most URM piers—in a predominant shear mode [Smith and Coull, 1991]. As a consequence, and similar to mixed RC-URM wall structures, the deformed shape of dual RC frame-wall buildings is modified and tends to be rather linear over the height of the structure [Paulay and Priestley, 1992].

If the masonry walls have a dominant flexural response, in the URM walls the inter-storey drift profile is rather constant over the height and the modification of the deformed shape is less accentuated. For modern URM buildings with RC slabs such a behaviour is, however, uncommon since the RC slabs connecting the walls feature a significant out-of-plane stiffness and strength and introduce therefore an important framing effect which leads to a more shear critical behaviour of the URM walls [Lang, 2002].

2.2. Advantages and drawbacks of adding RC walls in URM wall buildings

Fig. 4 compares failure mechanisms of a mixed RC-URM structure versus that of a URM building where shear deformations prevail. The presence of the RC wall in the retrofitted configuration leads, for the same level of inter-storey drift δ^* at the ground floor, to larger top displacements: $\Delta_{mixed} > \Delta_{URM}$. Consequently, the displacement capacity of mixed RC-URM wall structures is larger than that developed by shear dominated URM wall buildings. Furthermore, in

retrofit design, the URM walls with the smallest displacement capacity can be replaced by RC walls.

In addition, in such mixed systems, the strength degradation of shear dominated URM walls generally starts at drifts of around 0.3%-0.5%. At these drift levels, RC walls that are designed to develop a stable flexural behaviour are still in the pre-peak response. As a consequence, in mixed RC-URM wall structures the strength degradation of the URM walls can be somewhat compensated by the presence of the RC walls.

A drawback of the strategy is the increase in seismic mass related to the addition of RC walls to the structure. However, since large parts of the dead loads result from the weight of the RC slabs and the added RC walls in the retrofitted systems are usually few, the increase in total weight is, generally, less than 5%.

3. Numerical analysis of modern RC-URM wall buildings with RC slabs

Several modelling approaches are used for evaluating the seismic behaviour of mixed RC-URM wall structures, ranging from sophisticated strategies (shell-models) to more simplified approaches (macro-models). Although computer power increases continuously, it seems unlikely that shell-models will become a standard tool for the practically oriented analyses, as they require too much computational time.

Previous studies [Casoli, 2007; Paparo and Beyer, 2012] have also shown that numerical investigations using macro-models are sensitive to some modelling assumptions, such as the assumed effective stiffness of the members or the effective length of the coupling RC beams. In this paper, to validate two modelling approaches, a two-step validation procedure is used: *(i)* first, a detailed shell-model is assessed against the results from quasi-static cyclic tests. This model is then used to study additional parameters. *(ii)* The results of the macro-model are then compared and recommendations for the analysis of such mixed structures formulated. Before the presentation and comparison of the two modelling approaches, a brief overview of two quasi-static tests on two mixed RC-URM wall structures is outlined.

3.1. EPFL tests

Two mixed RC-URM substructures were tested under a quasi-static cyclic loading regime at the structural engineering laboratory at EPFL. Each of the two specimens comprised a two-storey RC wall coupled to a two-storey URM wall through two RC beams. The RC beams connecting the two walls represented the slabs in the reference structure.

The main difference between the two systems was the axial load applied at the top of the URM walls. For the first specimen (TU1), an axial load of 400 kN was applied and led to a shear dominant behaviour of the masonry. For the second test (TU2) the axial load was reduced to 200 kN in order to achieve a prevalent rocking behaviour. Fig. 2 shows the crack pattern of the two specimens after failure. In Sec. 3.4, the global force-displacement characteristics, as well as the inter-storey drift profile, will be introduced and compared with the analysis results. For further details on the EPFL tests, the reader is referred to Paparo and Beyer [2014].

3.2. Shell-element model

In the shell-element model, *(i)* URM walls are simulated by using the simplified micro-modelling approach [Lourenço, 1996] and *(ii)* RC walls and beams are represented by shell elements for the concrete, shell elements for the transverse reinforcements and trusses for the longitudinal reinforcements. The simulations are carried out using the software ATENA [Červenka *et al.*, 2010]. The mechanical properties, summarised in Table 1, were obtained from standard material tests, Paparo and Beyer [2014]. In the following, a description of the adopted mechanical properties is provided.

i) URM walls: Shell elements to which the SBETA constitutive model [Červenka *et al.*, 2008] is assigned are used to simulate the bricks as elastic in compression. Their tensile strength f_{tb} instead is limited to 1.4 MPa and the fracture energy G^I_b is set equal to 0.08 N/mm [Lourenço, 1996]. The mortar joints are modelled by zero-thickness contact interfaces with a Mohr-Coulomb failure criterion. The interface friction μ and cohesion c between mortar and bricks were obtained from standard triplet tests [EN 1052-3, 2002]. The interface tensile strength f_{tm} is calculated by considering a parabolic tension cut off:

$$f_{tm} = \frac{c}{2\mu} \tag{3.1}$$

The constitutive law assigned to the interfaces does not account for compression failure. As a consequence, the crushing of the masonry is not represented by the shell element model and,

therefore, the failure of the masonry cannot be fully captured. Thus, the shell element model is used to investigate the behaviour before failure, i.e. the shear-flexure interaction which develops between the RC and URM walls (Sec. 2.1) and the effective length of the RC beams.

As the software can only account for isotropic material behaviour, an equivalent E-modulus of the bricks, which lies in between the E-modulus of the bricks for loading parallel (E_{bx}) and orthogonal (E_{by}) to the perforations, is adopted (E_b). The different masonry E-modulus in the two directions of loading (E_{mv} and E_{mh}) can be matched by varying the normal and tangent interface stiffnesses (K_{nn} and K_{tt}). In the experimental program [Paparo and Beyer, 2014] the vertical masonry E-modulus E_{mv} was obtained from standard compression tests on masonry wallettes [EN 1052-1, 1998]. Compression tests in horizontal direction were not carried out. According to Beyer and Dazio [2012], who tested similar masonry walls under horizontal and vertical loads, the ratio E_{mh} / E_{mv} is estimated as 0.25. Hence it was assumed that $E_{mh} = 0.25\ E_{mv}$. As the investigated URM walls had dry head joints, the vertical masonry E-modulus (E_{mv}) can be related to the normal interface stiffness (K_{nn}) and the horizontal masonry E-modulus (E_{mh}) can be related to the tangent interface stiffness (K_{tt}). Simple compression tests with loading orthogonal and parallel to bed joints are simulated, allowing the calibration of K_{nn} and K_{tt} to obtain the two desired masonry E-moduli E_{mh} and E_{mv}.

The fracture energies of the joint interfaces (G^I_f and G^{II}_f) were not determined within this project [Paparo and Beyer, 2014]. The interface Mode II fracture energy G^{II}_f is assumed to be equal to 0.50 N/mm, according to Beyer and Dazio [2012]. Since for the interface Mode I fracture energy G^I_f no experimental results for hollow clay bricks were found, it is assumed that the ratio G^I_f/G^{II}_f

is equal to the ratio f_{tm}/c [Reyes *et al*., 2008]. Since G^I_f and G^{II}_f were not determined directly from material tests, sensitivity analyses of their influence to the response of single URM walls were carried out. Also according to Lourenço [1996], it was found that the assumed values of G^I_f and G^{II}_f are parameters which do not strongly affect the results of the analyses.

ii) RC walls and beams: The concrete behaviour of RC walls and beams is modelled using shell elements in conjunction with the SBETA model [Červenka *et al.*, 2008]. The concrete behaviour in compression is parabolic up to the cylinder compressive values f_c and f_{cc}. The cylinder compressive value f_c is used for modelling the unconfined concrete in the RC walls. In the boundary elements of the RC walls and in the RC beams, the concrete compressive strength adopted is f_{cc}. This value accounts for the effect of the confinement and is calculated according to Mander *et al.* [1988]. After the peak stresses f_c and f_{cc}, the softening law of the concrete would be linearly descending but this was not reached in any of the analyses. The concrete behaviour in tension is modelled using a linear-elastic relation until the tensile strength (f_{tc}). After the stress peak f_{tc}, the concrete is modelled with an exponential tension softening law. The concrete tensile strength f_{tc} was experimentally determined from double punch tests on half cylinders [Chen, 1970]. A bilinear stress-strain relation is adopted for the reinforcing bars in conjunction with (*i*) truss elements for representing longitudinal reinforcements and (*ii*) shells for representing transverse smeared reinforcements. Perfect bond between steel and concrete is always assumed.

3.3. Macro-element model

The macro-model strategy consists of modelling each structural member as single elements which are then assembled to an equivalent frame. The macro-element developed by Penna *et al*.

[2013] is used to describe the behaviour of masonry walls. Timoshenko beams characterised by an elasto-plastic law represent RC members [Cattari and Lagomarsino, 2013]. The simulations are carried out with the software TREMURI [Lagomarsino *et al.*, 2009; Lagomarsino *et al.*; 2013, Penna *et al*., 2013].

The adopted mechanical properties are summarised in Table 2. The equivalent friction and cohesion parameters for masonry piers (μ_{eq} and c_{eq}) are computed as follows:

Step1) Calculation of the shear strength: For single masonry walls, Penna *et al*. [2013] proposed to set the equivalent friction and cohesion (*i*) on the basis of the strength criterion which is representative of the expected failure and (*ii*) assuming the axial force *N* acting on the section. For multi-storey (mixed RC-URM and plain URM) wall buildings with RC slabs, Mandirola [2014] used the same approach and set μ_{eq} and c_{eq} (*i*) on the basis of the shear criterion which represents the expected shear failure and (*ii*) assuming the axial force *N* at the base of the URM walls considering the gravity loads only. The latter assumption means that the calibration is made without taking into account the variation of the axial force in the URM walls due to the floor level and the load transferred by the RC slabs.

As the objective of the paper is to provide practical guidelines for setting up models by using standard material tests only, the approach proposed by Mandirola [2014] is followed herein. Note that, in a multi-storey building, the approach would require different values of μ_{eq} and c_{eq} depending on the floor level to account for the variation of axial force over the height of the building. However, since in the top storeys the URM walls are dominated by rocking

deformations because of the low axial force acting on the URM walls, a variation of μ_{eq} and c_{eq} is unlikely to affect the results significantly.

Step 2) Calculation of μ_{eq} and c_{eq}: In the macro-element developed by Penna *et al*. [2013], the shear strength of a masonry wall V_{sh} is the sum of the friction component V_{μ} and the cohesion component V_c:

$$V_{sh} = V_{\mu} + V_c \tag{3.2}$$

The equivalent friction and cohesion parameters μ_{eq} and c_{eq} can be found by assigning half of the shear strength to the friction component V_{μ} and half of the shear strength to the cohesion component V_c:

$$0.5 \cdot V_{sh} = V_{\mu} = \mu_{eq} \cdot N \tag{3.3a}$$

$$0.5 \cdot V_{sh} = V_c = c_{eq} \cdot A_{gross} \tag{3.3b}$$

Note that (*i*) the cohesion component V_c is determined considering the gross section area A_{gross} and that (*ii*), for URM walls with shear behaviour, plastic displacements occur when the shear force V is bigger than the friction component (V_{μ}). The assignment of 50% of the total shear (V_{sh}) to cohesive and friction components is chosen on the basis of the experimental results. In fact, in the hysteretic behaviour of TU1 and TU2, the stiffness degradation in the masonry walls

starts for values of shear forces V equal to around 50% V_{sh}. The force-displacement results of two quasi-static cyclic tests [Petry and Beyer, 2014a] on URM walls exhibiting dominant shear behaviour are used to validate the approach for the calculation of μ_{eq} and c_{eq}. The comparison (Fig. 5) shows that the TREMURI models with the proposed values of μ_{eq} and c_{eq} provide good estimates of the stiffness degradation in the pre-peak response and of the dissipated energy (β = 0.25).

Concerning the calculation of the shear strength of the masonry wall, Penna *et al*. [2013] propose to use the strength criterion which is representative of the expected failure. In this case, the strength of the masonry panel is calculated by using the shear strength criterion which accounts for the brick tensile strength [Mann and Müller, 1982]:

$$V_{sh} = lt\frac{f_{tb}}{2.3(1+\alpha_v)}\sqrt{1+\frac{N}{ltf_{tb}}} \tag{3.4}$$

where l and t are the length and the thickness of the masonry wall, N the axial force acting on section and f_{tb} the brick tensile strength. $(1+\alpha_v) = (1+H_{CF}/l)$ is a correction coefficient proposed by Magenes and Calvi [1997] to account for the effect of complex stress distribution. H_{CF} is the height of the contra-flexure point of the masonry wall. According to such a calibration, for TU1 the shear strength V_{sh} is equal to 141 kN (N = 460 kN) and for TU2 the shear strength V_{sh} is equal to 123 kN (N = 260 kN). The experiments have shown that, for TU1 and TU2, H_{CF} can be assumed equal to the storey height. The tensile strength of the brick, f_{tb}, is set equal to 1.27 MPa

according to Petry and Beyer [2014a] who tested masonry walls similar to those herein considered.

In Table 2, the adopted E-modulus corresponds to the vertical masonry E-modulus (E_{mv}) obtained from standard compression tests on masonry wallettes [EN 1052-1, 1998], see Sec. 3.2. The shear modulus (G_m) is calculated from the E-modulus E_{mh} (compression parallel to bed-joints, see Sec. 3.2):

$$G_m = \frac{E_{mh}}{2 \cdot (1 + \nu_M)} = \frac{(0.25 \cdot E_{mv})}{2 \cdot (1 + \nu_M)} \tag{3.5}$$

ν_M is the Poisson ratio of the masonry wall which was found to be equal to 0.18 according to EN 1052-1 [1998].

For the construction of the macro-model, additional assumptions on the stiffness and deformation capacity of the elements are required:

i) Stiffness of URM walls: The stiffness of URM walls corresponds to the uncracked stiffness of the section. For the shear damage model, non-linear plastic deformations in the pre-peak response are taken into account by the effect of the shear deformability parameter Gc_t [Penna *et al.*, 2013]. The latter is set equal to one so that, at peak strength (V_{sh}), the total horizontal displacement u_{tot} is 1.5 times the elastic one u_{el}:

$$u_{tot} = 1.5 u_{el} \tag{3.6}$$

with $u_{el} = V_{sh} h / (G_m l t)$. h, l, t are the height, length, thickness of the wall. For the flexural behaviour, non-linear elastic deformations are taken into account in terms of kinematic variables (rotation and vertical displacement of the section). A no tension model is attributed to the zero-length springs in which flexural and axial deformations are lumped [Penna *et al.*, 2013].

ii) Softening parameter β: The parameter β, which describes the softening post-peak response of the URM walls, is here set equal to zero. This means that the macro-element does not display any strength degradation after the peak.

iii) Failure criterion for URM walls: The failure criterion follows the formulation proposed by EN 1998-3 [2005] in which the near collapse (NC) inter-storey drift δ_u of a masonry wall depends on its failure mechanism:

For shear failure $\delta_u = 0.53\%$ (3.7a)

For flexural failure $\delta_u = 1.07\% \cdot (H_{CF} / L)$ (3.7b)

For flexural failure, the near collapse drift is also dependant on the ratio H_{CF}/L (height of the contra-flexure point over length of the pier). Although the pier's displacement capacity is defined as horizontal load failure, tests have shown that URM walls lose their vertical load bearing capacity soon after the horizontal load failure [Petry and Beyer, 2014b]. Once the first URM pier

fails, it is assumed that the system reaches its ultimate displacement capacity. The inter-storey drift δ is calculated as follows:

$$\delta = \frac{\Delta_i - \Delta_j}{h} \tag{3.8}$$

where Δ_i and Δ_j are the horizontal displacements of the beams below and above the considered wall and h the height of the wall.

iv) Stiffness of RC members: Experiments on mixed RC-URM wall structures [Paparo and Beyer, 2014; Beyer *et al*., 2014] have shown that the RC walls crack only in the first storey, while the above storeys feature just thin cracks, mainly in the construction joints connecting walls and slabs (or beams). As a consequence, the reduction of stiffness according to Priestley *et al.* [2007] is applied to the first storey of the RC walls and to the RC beams. This reduction is taken into account by considering the effective stiffness EI_e:

$$EI_e = \frac{M_N}{\varphi_y} \tag{3.9}$$

where M_N is the nominal yield moment, calculated considering the axial force acting at the base of the wall before applying the horizontal load, and φ_y is the nominal yield curvature, which is equal to $C\varepsilon_y/l_w$. C is a constant depending on the geometrical properties of the section; ε_y is the yield strain of the longitudinal reinforcing bars and l_w is the length of the wall. To account for the presence of thin cracks in construction joints between the RC walls above the first storey and

the slabs (or beams), the concrete E-modulus of the RC walls above the first storey is reduced by 50%. The latter assumption is considered applicable if (*i*) the mean longitudinal reinforcement ratio of the RC walls is within the range of 0.2% and 4.0% and if (*ii*) the RC walls are built between floor levels and their longitudinal reinforcements pass across the slabs, as it is generally the case for mixed RC-URM structures representative for residential buildings in Switzerland.

v) Axial stiffness of RC beams: The RC beams are modelled with infinite axial stiffness to guarantee that the walls at each floor displace horizontally by the same amount.

vi) Failure criterion for RC members: All RC elements are designed to form a ductile flexural mechanism. The ultimate chord rotation θ_u of RC members is estimated according to EN 1998-3 [2005]. However, the deformation capacity of RC members developing a stable flexural response is much larger than that of URM walls. In all the analyses presented in this paper, the RC elements do not reach their deformation capacity.

vii) Effective length of the RC beams: In the macro-model the user can control the effective length of the RC beams (L_{be}) by introducing rigid offsets. To account for the curvature penetration of RC beams into URM walls, the deformable part is increased by its section depth h_b where the beam spans into an URM wall [Priestley *et al.,* 2007]. In case of beams connecting two URM walls one obtains as length of the deformable part of the beam:

$$L_{be} = h_b + L_b + h_b \tag{3.10a}$$

where L_b is the clear distance between the ends of the two walls. If the beam spans one URM and one RC wall (as represented in Fig. 6bone obtains:

$$L_{be} = h_b + L_b \tag{3.10b}$$

The effective length of the beams influences their stiffness and therefore their shear force, which lead to the variation of axial force at the base of the walls. Fig. 6a compares the variation of the axial force at the base of the URM wall for macro-models with different effective lengths to the data obtained from TU2. Results indicate that the best match in terms of variation of axial force at the base of the URM wall is, indeed, obtained for L_{be} according to Eq. (3.10).

A parametric study comparing the response between the shell-model and the macro-model is carried out. The investigated parameters are *(i)* the axial load applied at the top of the two storeys of the URM wall and *(ii)* the strength of the RC beams (Fig. 6b and 7). The objective is to ascertain if the estimation of L_{be} according to Eq. (3.10) in the macro-model can be used also for different configurations of masonry structures. The study is carried out by comparing the variation of axial stress at the base of the URM wall since such a variation is directly related to the assumed deformable length of the RC beams (L_{be}). The results confirm that in the macro-model the effective length of the RC beams is accurately estimated by Eq. (3.10) also for different strengths of the RC beams (ρ_b = 0.6% - 1.2%) and different axial load ratios of the URM walls (σ_0/f_{cM} = 0.2 - 0.6).

3.4. Comparison of the numerical and experimental results

Comparison between the two numerical models and the experiments is made by analysing:

i) The distribution of the base shear among the walls, to assess the influence of the relative stiffness of the members;

ii) The distribution of the axial force between the walls, to check the assumptions of the effective length of the RC beams;

iii) The inter-storey drift profile over the height of the structure, to ascertain the predicted deformed shapes.

When comparing the numerical to the experimental results, it is assessed which of the two models predicts the experimentally obtained values better. Further it is assessed whether the numerical models can capture the trends of the experimental results with increasing displacement demand. The numerical results are not benchmarked against the experimental results in absolute terms since, for example, small unintended variations in the axial load that was applied during the test might falsify the picture.

Fig. 8a and 8b show that the shear carried by the walls is estimated rather accurately by both numerical approaches. Note, however, that with regard to the shear carried by the RC walls, the two models performed differently. *(i)* The macro-model approximates the force-displacement response of the RC walls with a bilinear relation which initial slope corresponds to the effective . As a consequence, it does not capture the stiffness degradation of the RC members due to

cracking and the onset of yielding of the longitudinal bars and therefore underestimates the shear forces carried by the RC walls before yielding. *(ii)* The shell-model, instead, captures the stiffness degradation of the RC members.

For TU1 there are some discrepancies in the distribution of the axial force between the models and the experimental results (Fig. 8c). During testing of TU1, the total axial load applied at the top of the URM wall varied with around 30 kN while in the numerical analyses the axial load was kept constant. As a consequence, the variation of axial force that is due to the variation of the axial load applied at the top of the URM wall is not taken into account in the simulations. On the other hand, for TU2 (Fig. 8d), the axial load applied at the top of the URM wall was constant throughout the testing procedure and the difference between experiments and analytical results is small.

During the testing of TU1 and TU2, the inter-storey drift δ of the first storey was almost equal to that of the second storey and the same trend is found from the simulations (Fig. 9a and 9b). Fig. 9c and 9d represent the ratio between the inter-storey drift and the average drift. Except for absolute average drifts smaller than 0.1%, the comparison between experiments and simulations is satisfactory and differences smaller than 15% are found. The evaluation of the displacement capacity, calculated only with the macro-model, gives good results although the displacement capacity of the structure is somewhat overestimated for the negative direction of loading. In Fig. 8 and 9 the numerical simulations performed with the macro-model are stopped when the failure criterion is attained. In addition, the two numerical strategies are able to capture the prevailing shear and flexure damage modes that occurred over the height of the URM walls.

The macro-model can be used for practically oriented analyses of complete mixed RC-URM wall structures and, following the indications proposed in Sec. 3.3, relative accurate results with a limited computational effort can be obtained. The shell-element approach instead, can be adopted for detailed analyses of the mechanical behaviour of small substructures to give a better understanding about their local behaviour. Moreover, the shell-element approach can be used when an irregular arrangement of openings does not allow the definition of an equivalent frame in the macro-model approach or when the URM walls have not sufficiently large dimensions to be treated as macro-elements [Lourenço, 1996]. However, due to the regularity of the herein analysed mixed buildings, the macro-modelling technique can be generally used and is the most suitable tool for practically oriented analyses of such buildings.

4. Application to four buildings

One reference structure and three retrofit solutions (Fig. 10) are compared to exemplify the benefits of retrofitting URM buildings by replacing or adding RC walls. The reference structure is a four-storey building composed of three URM walls. The adopted geometrical configuration leads to a shear failure mechanism at the bottom storey. In case study 1 one URM wall is replaced by one RC wall of the same length. Case study 2 represents the retrofit design made by the insertion of one RC wall which is parallel but not in the same plane of the other URM walls. As a consequence, in the numerical simulations the RC wall is connected to the URM structure with axially rigid links with zero moment capacity at each floor as represented in Fig. 10c. In case study 3 two slender RC walls are added to the original URM building. Fig. 10 shows the elevation of the four structures and the lateral load pattern applied. The thickness of the walls is

always equal to 0.20 m. Two-dimensional simulations are carried out and RC beams 0.25x0.60 m represent the slabs. The thickness of the RC beams is three times that of the walls [Priestley *et al.*, 2007] and the free span of the RC beams is 1.05 m. The axial stress ratio σ_0/f_{cM} at the base of the URM walls is around 0.14. All RC walls and slabs are designed such that the URM walls fail before any RC element. RC member's longitudinal reinforcement ratios are listed in Table 3; the shear reinforcement of RC walls and beams are designed to prevent shear failure. The total masses of the buildings are proportional to the sum of the length of the walls, that is 180 t for the reference structure and case study 1; 240 t for case studies 2 and 3.

The reference structure and case study 1 (Fig. 10a and 10b) are also analysed considering a lower coupling provided by the RC beams (ρ_b equal to 0.20%). The objective is to decrease the coupling effect provided by the RC beams and achieve dominant rocking behaviour of the URM walls. This configuration will show that for buildings with rocking URM walls the increase in displacement capacity after the retrofitting is smaller than for buildings where the URM walls develop a dominant shear behaviour.

The analyses are carried out with the macro-model following the indications described in Sec. 3.3. μ_{eq} and c_{eq}, the equivalent friction and cohesion coefficients, are equal to 0.18 [-] and 0.17 MPa respectively. The analyses are performed until the structures reach their Significant Damage (SD) limit state, which corresponds to the instant when the first URM wall reaches the target inter-storey drift capacity δ_{cap}. For walls failing in shear, the inter-storey drift capacity at the SD limit state is assumed as 0.4% [EN 1998-3, 2005]. For URM walls failing in flexure, their inter-

storey drift capacity δ_{cap} is set equal to 0.8% H_{CF}/L [EN 1998-3, 2005]. The inter-storey drift demand of each wall (δ_D) is calculated as follows:

$$\delta_D = \frac{\Delta_i - \Delta_j}{h} - \theta_i \tag{4.1}$$

where Δ_i and Δ_j are the horizontal displacements of the beams below and above the considered wall, h the height of the wall and θ_i the rotation of beam below the wall. Comparisons will be carried out by analysing the capacity curves (Sec. 4.1) and the results from the N2 method (Sec. 4.2).

4.1. Capacity curves

Fig. 11 represents the capacity curves of the four case studies for the two directions of loading. Besides the augmentation in strength, there is an increase in average drift capacity between approximately 50-60% (see also Table 4). As outlined in Sec. 2, the RC walls change the deformed shape and avoid a concentration of damage in the first storey.

Case study 1 is not plan-symmetric and its response changes whether the structure is pushed towards one direction or another (Fig. 11a). URM walls are, in fact, much more sensitive to the variation of the axial force if compared to RC walls with respect to their stiffness, displacement and strength capacity. Since URM wall 1 and the RC wall are flanked by beams only from one direction (Fig. 10b), the axial force at their base changes depending on the loading direction.

Fig. 12 represents the force-displacement relation for the reference structure and case study 1 when the longitudinal reinforcement ratio ρ_b of the beams is reduced to 0.20%. This configuration represents the effect of the retrofitting technique when the URM walls develop mainly a rocking behaviour. Since the addition of the RC wall does not particularly change the deformed shape of the structure, there is no significant increase in displacement capacity. In Fig. 12, the displacement and strength capacities of the retrofitted configuration change depending on the loading direction since the retrofitted configuration is not plan symmetric (Fig. 10a).

4.2. N2 method

The objective of structural engineers designing a retrofit intervention is that the retrofitted structure can withstand a larger seismic hazard than the original building. In codes the seismic hazard is typically expressed by the peak ground acceleration (PGA), which scales the shape of the design spectrum. Since retrofit interventions affect stiffness, strength and deformation capacity, the resulting increase in maximum peak ground acceleration (PGA_{max}) that the structure can withstand is evaluated by the N2 method. The method evaluates the so called "performance point", which is found by comparing the capacity curve of the equivalent bi-linear single-degree of freedom (SDOF) system with the seismic demand [Fajfar, 2000]. From the pushover curve of the multi-degree of freedom system (actual MDOF response), the force-displacement response of the SDOF system (actual SDOF response) is computed according to EN 1998-1 [2004], Fig. 13a. The bi-linear approximation of the SDOF's force-displacement response is then constructed using the proposed criteria of Table 5 (see also Fig. 13b) and the performance point of the structures is computed according to EN 1998-1 [2004].

Besides the comparison of PGA_{max}, the other quantities representing the seismic behaviour of the bilinear approximation of the equivalent SDOF systems (T^*, Δ^*_y, Δ^*_u, μ^*, F^*_b) are summarised in Table 6. In the analyses, the seismic demand is represented by an acceleration design spectrum of soil class C (T_b = 0.2 s; T_c = 0.6 s and T_d = 2 s [EN 1998-1, 2004]). Note that for all the structures the equivalent period T^* (period of the equivalent SDOF system) is lower than T_c, as it is generally the case for URM structures. As for all the configurations $T^* < T_c$ = 0.6 s, the performance point of the equivalent SDOF system Δ^*_u is calculated as follows [EN 1998-1, 2004]:

$$\Delta^*_u = \frac{\Delta^*_{et}}{q_u}\left(1+(q_u-1)\frac{T_c}{T^*}\right) \geq \Delta^*_{et} \tag{4.2}$$

where Δ^*_{et} is the performance point of the SDOF system with period T^* and unlimited elastic behaviour:

$$\Delta^*_{et} = S_a(T^*)\left(\frac{T^*}{2\pi}\right)^2 \tag{4.3}$$

q_u is the ratio between the peak acceleration in the structure with unlimited elastic behaviour and in that with limited strength. $S_a(T^*)$ is the elastic acceleration response spectrum at the equivalent period T^*. Fig. 14a shows the used acceleration design spectrum for PGA = 1 m/s^2, whereas Fig. 14b to 14f represent the identification of the performance point in the acceleration-displacement response spectra for the maximum PGA that the structures withstand (PGA_{max}).

For the three case studies, the system's yield displacements Δ^*_y are between 1.15 to 1.45 times the one of the reference structure. The ultimate displacements Δ^*_u increase between 1.50 and 1.60 times, mainly because of the change in displacement profile due to the insertion of RC walls. As a result, the ductility of the system μ^* increases between 5% and 30%. The base shear capacity of the equivalent SDOF system (F^*_b) rises for all the case studies. In case study 3 the increase in base shear is larger than for the other configurations due to the larger frame effect developed by the presence of the two RC walls. As a result of the increase displacement and force capacity, the maximum *PGA* that the structures can sustain (PGA_{max}) rises between 140-170%.

5. Conclusions and outlook

The article presented a retrofit technique for modern URM buildings connected by RC slabs by adding or replacing RC walls to the original structure. The study targeted structures where the RC members are designed to fail for larger displacement demands than the URM walls. Mixed RC-URM buildings in which the RC members are not capacity-designed were not herein considered. The advantages of this retrofitting technique are related to (*i)* an increase in strength capacity and *(ii)* a change of the deformed shape. The latter provides a failure mechanism with larger top displacements for the same level of inter-storey drift at the ground floor (Fig. 4).

In order to analyse such structures, two computational strategies were presented, namely a shell-model and a macro-model approach. The results of the two techniques were compared against experimental results and judged satisfactory. The macro-model, although requiring limited

computational efforts, was capable of representing all the main features of the seismic behaviour of mixed RC-URM wall structures: *(i)* distribution of the reaction forces between the walls at peak strength, *(ii)* evaluation of the inter-storey drift profile over the height of the structure, *(iii)* evaluation of the ultimate displacement capacity and *(iv)* damage modes that occurred in the URM walls. As a consequence a macro-element model, which follows the indications proposed in Sec. 3.3, is particularly recommended for practically oriented analysis of complete mixed RC-URM wall structures. A shell-model approach, instead, can be adopted for analysing in detail the mechanical behaviour of small substructures where more refined analyses are needed.

The case studies evaluated the benefits in terms of design quantities: the increase in displacement capacity ranged between 50% and 60% and the increase in PGA_{max} was between 40% and 70%. The displacement ductility μ^* increased between 5% and 30%.

The RC wall length, as well as its reinforcement ratio, was kept constant. Further studies will address the effects of varying the RC wall length and its reinforcement ratio with the objective of optimising the efficiency of the retrofitting technique.

Acknowledgements

The authors thank Chris Genis for proofreading the manuscript.

References

Beyer, K. and Dazio, A. [2012] "Quasi-Static Cyclic Tests on Masonry Spandrels," Earthquake spectra, 28(3), 907-929.

Beyer, K., Tondelli, M., Petry, S. and Peloso, S. [2014] "Dynamic testing of a 4-storey building with reinforced concrete and unreinforced masonry walls", submitted to *Bulletin of Earthquake Engineering*.

Casoli, D. [2007] "Assessment of existing mixed RC-Masonry structures and strengthening by RC shear walls," Pavia, Italy.

Cattari, S. and Lagomarsino, S. [2013] "Seismic design of mixed masonry-reinforced concrete buildings by non-linear static analyses," *Earthquakes and Structures*, Vol. 4, N°3.

Červenka, J. and Papanikolaou, V.K. [2008] "Three dimensional combined fracture-plastic material model for concrete," *International Journal of Plasticity*, 24, 2192-2220.

Červenka, V., Jendele, L. and Červenka, J. [2010] "Atena - Computer Program for Nonlinear Finite Element Analysis of Reinforced Concrete Structures," *Theory and User Manual*, Prague, Czech Republic.

Chen, W. [1970] "Double punch test for tensile strength of concrete," *ACI Journal*, 67, 993-995.

EN 1052-1 [1998] *Eurocode 6: Methods of test for masonry – Part 1: Determination of the compressive strength*, CEN, Brussels.

EN 1052-3 [2002] *Eurocode 6: Methods of test for masonry – Part 3: Determination of the initial shear strength*, CEN, Brussels.

EN 1992-1-1 [2004] *Eurocode 2: Design of concrete structures – Part 1-1: General rules and rules for buildings*, CEN, Brussels.

EN 1996-1 [2005] *Eurocode 6: Design of masonry structures – Part 1: General rules for reinforced and unreinforced masonry structures*, CEN, Brussels.

EN 1998-1 [2004] *Eurocode 8: Design of structures for earthquake resistance* – Part 1: *General rules, seismic actions and rules for buildings*, CEN, Brussels.

EN 1998-3 [2005] *Eurocode 8: Design of structures for earthquake resistance* – Part 3: *Assessment and retrofitting of buildings*, CEN, Brussels

Fajfar, P. [2000] "A non linear analysis method for performance-based seismic design," *Earthquake Spectra*, 16(3), 573-591.

Jurukovski, D., Krstevska, L., Alessi, R., Diotallevi, P.P., Merli, M. and Zarri, F. [1992] "Shaking table tests of three four-storey brick masonry models: original and strengthened by RC core and by RC jackets," *Proc. of 10th World Conference on earthquake Engineering*, Madrid, Spain.

Lagomarsino, S., Penna, A., Galasco, A. and Cattari, S. [2009] "Tremuri User Guide," Genova, Italy.

Lagomarsino, S., Penna, A., Galasco, A. and Cattari S. [2013] "TREMURI program: an equivalent frame model for the non-linear seismic analysis of masonry buildings," *Engineering Structures*, 6, 1787–1799.

Lang, K. [2002] "Seismic vulnerability of existing buildings," Ph.D. thesis, ETH Zurich, Zurich, Switzerland.

Lourenço, P.B. [1996] "Computational Strategies for Masonry Structures," Ph.D. thesis, Delft University, Delft, The Netherlands.

Magenes, G. and Calvi, G.M. [1997] "In-plane seismic response of brick masonry walls," Earthquake Engineering and Structural Dynamics, 26, 1091-1112.

Magenes, G. [2006] "Masonry building design in seismic areas: recent experiences and prospects form and european standpoint," Keynote address, *Proc of 1st European Conference on Earthquake Engineering and Seismology*, Geneva, Switzerland.

Mander, J.B., Priestley, M.N.J. and Park, R. [1988] "Theoretical stress-strain model for confined concrete," ASCE Journal of Structural Engineering, 114(8), 1804-1826.

Mandirola, M. [2014] "Non-linear macroelement modelling of experimental tests on masonry building specimens with rigid diaphragms," Pavia, Italy.

Mann, W. and Müller, H. [1982] "Failure of shear-stressed masonry: an enlarged theory, tests and application to shear walls," *Proc. of the British Ceramic Society*, 30, 223-235.

Paparo, A. and Beyer, K. [2012] "Pushover Analyses of Mixed RC-URM wall structures," *Proc. of 15th World Conference on earthquake Engineering*, Lisbon, Portugal.

Paparo, A. and Beyer, K. [2014] "Quasi-static tests of two mixed reinforced concrete – unreinforced masonry wall structures," *Engineering Structures*, 71, 201–211.

Paulay, T. and Priestley, M.N.J. [1992] *Seismic design of reinforced concrete and masonry buildings*, John Wiley & Sons, Inc., New York.

Penna, A., Lagomarsino, S. and Galasco, A. [2013] "A nonlinear macro-element model for the seismic analyses of masonry buildings," Earthquake Engineering and Structural Dynamics, 10.1002/eqe.2335.

Petry, S. and Beyer, K. [2014a] "Cyclic test data of six unreinforced masonry walls with different boundary conditions," *Earthquake Spectra*.

Petry, S. and Beyer, K. [2014b] "Influence of boundary conditions and size effect on the drift capacity of URM walls," *Engineering Structures*, 65, 76-88.

Reyes, E., Casati, M.J. and Galvez, J.C [2008] "Cohesive crack model for mixed mode fracture of brick masonry," International Journal of Fracture, 151:29-55.

Priestley, M.J.N., Calvi, G.M. and Kowalsky, M.J. [2007] *Displacement-Based Seismic Design of Structures*, IUSS Press, Pavia, Italy.

SIA 162/1 [1995] *Building code, Swiss Society of Engineers and Architects (SIA): Ouvreages en béton – Essais des matériaux*, SIA, Zurich.

Smith, B.S. and Coull, A. [1991] *Tall building structures: analysis and design*, John Wiley & Sons, Inc., New York.

Tomaževič, M., Modena, C., Velechovsky, T. and Weiss, P. [1990] "The effect of reinforcement on the seismic behaviour of masonry buildings with mixed structural systems: an experimental study," *Proc. of 9th European Conference on earthquake Engineering*, Moscow, Russia.

FIGURE 1 Deformation pattern and inter-storey drift profile due to lateral forces of a single URM wall with dominant shear behaviour (a), a single RC wall with dominant flexure behaviour (b) and a mixed RC-URM structure (c).

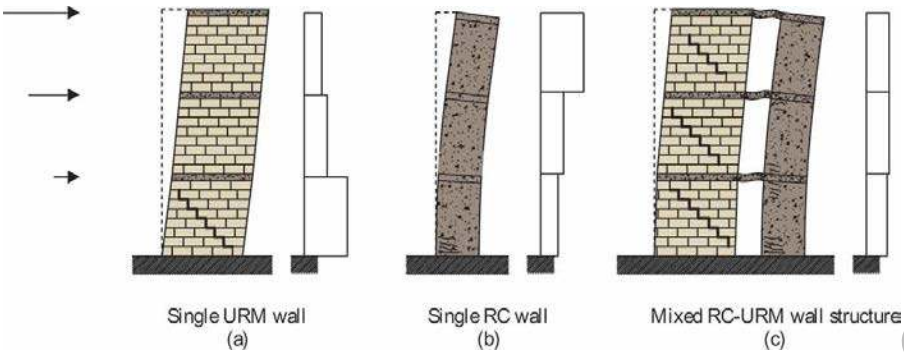

FIGURE 2 EPFL tests on two mixed RC-URM wall substructures: crack pattern after failure. (a): TU1. (b): TU2 [Paparo and Beyer, 2014].

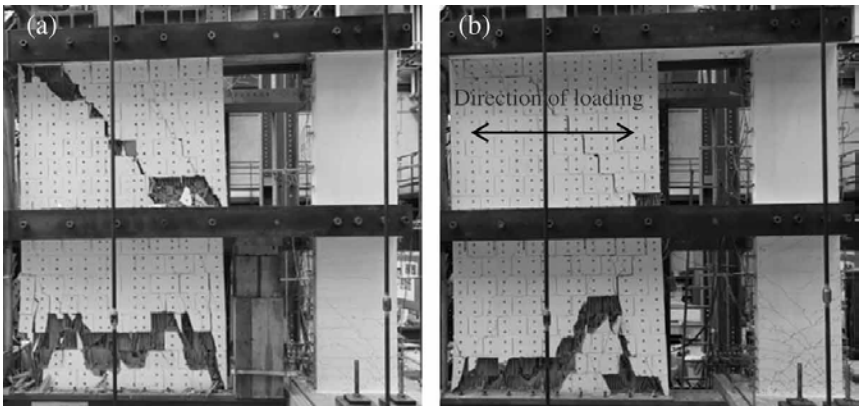

FIGURE 3 Crack pattern in a four-storey mixed RC-URM wall structure, from Beyer *et al.* [2014].

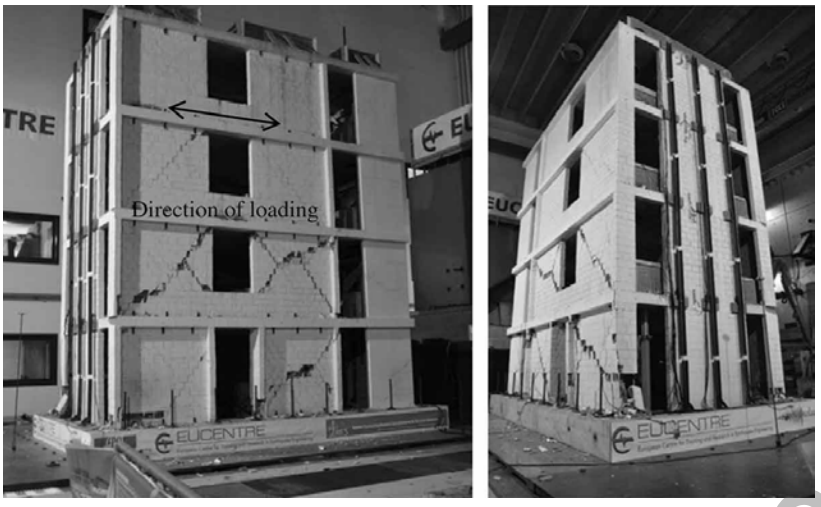

FIGURE 4 Deformation capacity, for the same level of inter-storey drift δ^*, of a mixed RC-URM structure (a) and a shear dominated URM building (b).

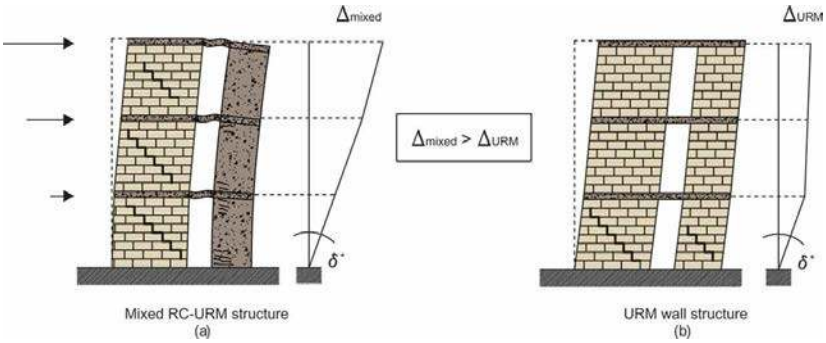

FIGURE 5 Comparison of the force-displacement curves obtained from in-plane cyclic tests [Petry and Beyer, 2014a] and numerical simulations.

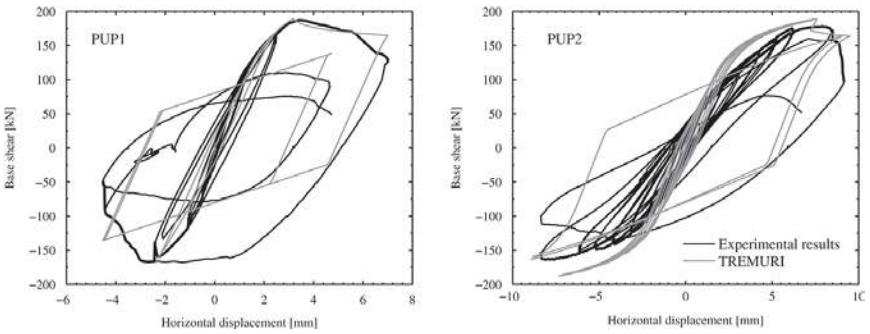

FIGURE 6 Effective length (L_{be}) of the RC beams in the macro-model. (a): comparison of the variation of the axial force at the base of the URM wall between TU2 (experiment) and macro-models with different effective lengths. (b): model for the parametric study.

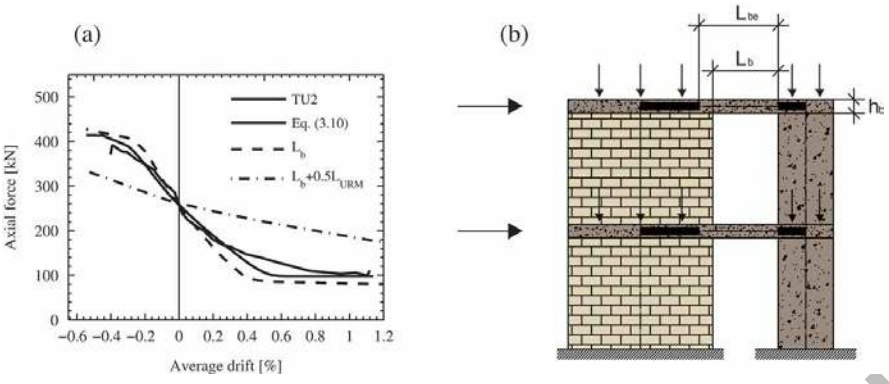

FIGURE 7 Effective length (L_{be}) to be adopted in the macro-model, parametric study. Variation of axial stress ratio for different axial loads applied to the URM wall (σ_0/f_n) and different beam reinforcement ratios (ρ_b).

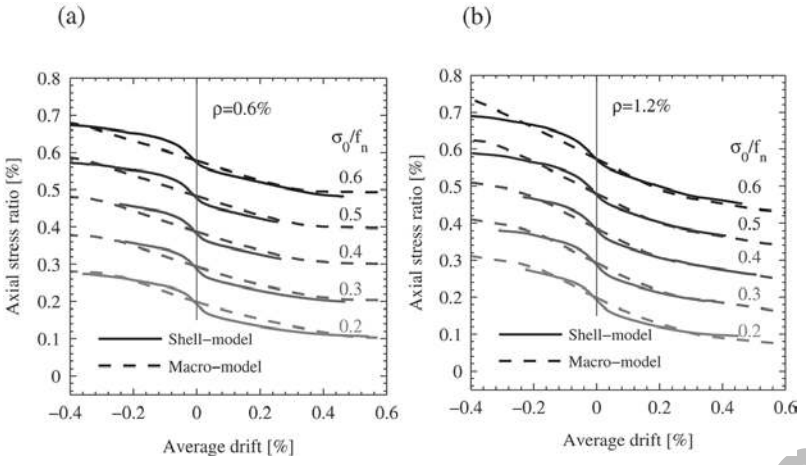

FIGURE 8 Distribution of the reaction forces between the two walls. (a), (b): base shear; (c), (d): axial force.

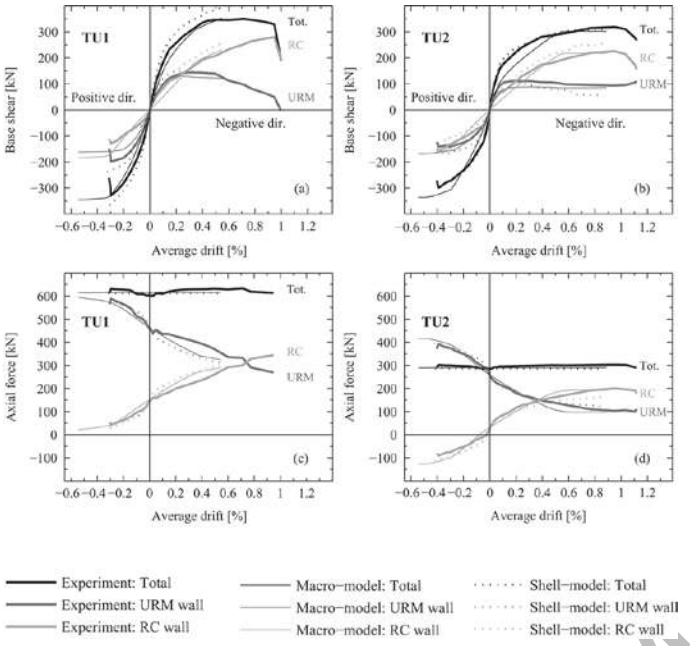

FIGURE 9 (a), (b): inter-storey drift profile over the height of the structure; (c), (d): ratio inter-storey drift-average drift.

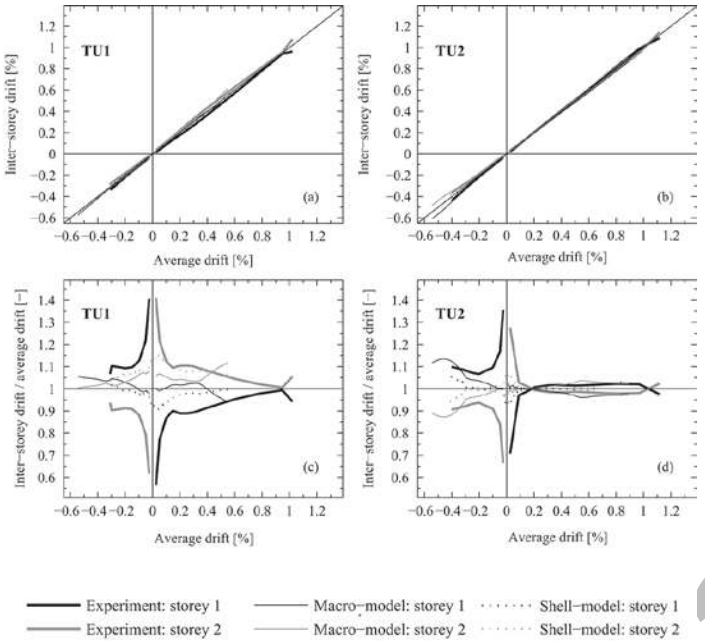

FIGURE 10 (a): reference URM structure; (b): case study 1; (c): case study 2; (d): case study 3. All dimensions in m. All RC beams have a clear span of 1.05 m.

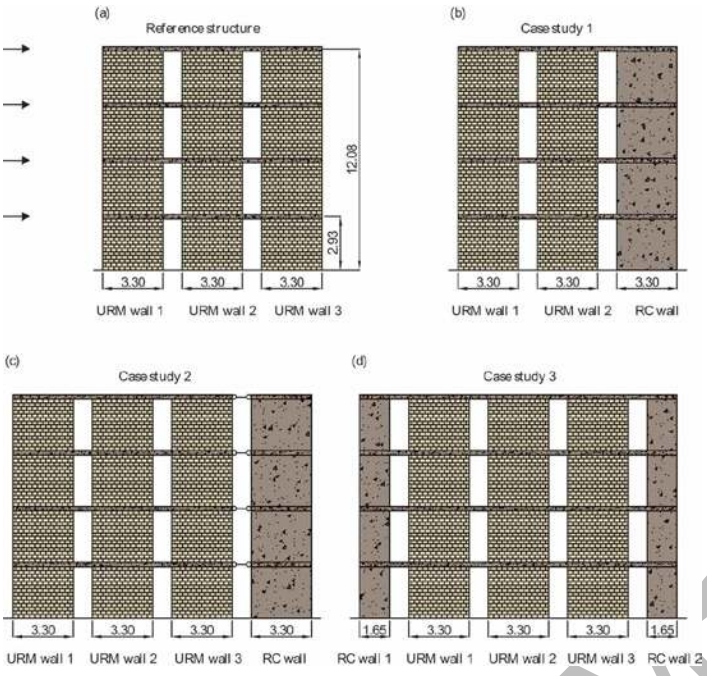

FIGURE 11 Force-displacement relations: reference URM structure and retrofitted configurations; squares indicate yielding of the RC walls.

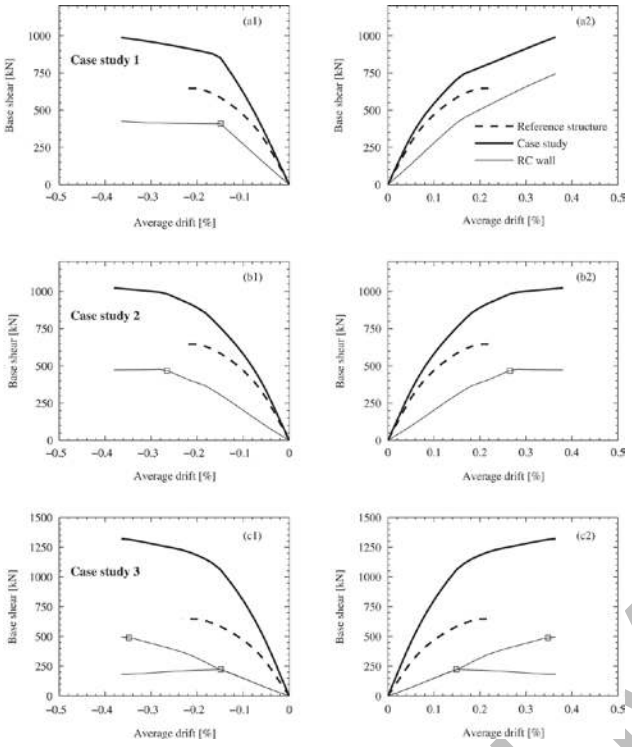

FIGURE 12 Force-displacement relations: reference structure and case study 1 when the URM walls have a dominant flexural behaviour. Squares indicate yielding of the RC walls.

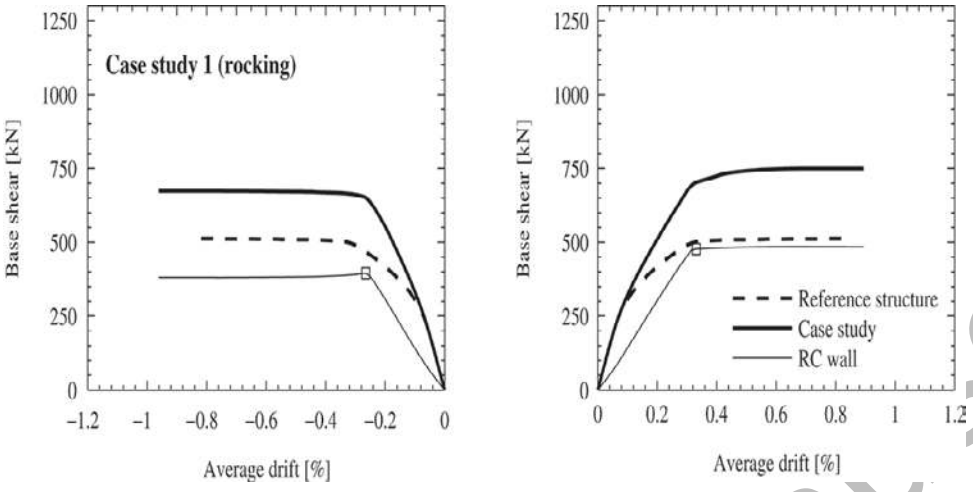

FIGURE 13 Mixed RC-URM wall structure, force-displacement curve. (a): actual MDOF and SDOF responses; (b): actual SDOF response and equivalent SDOF system.

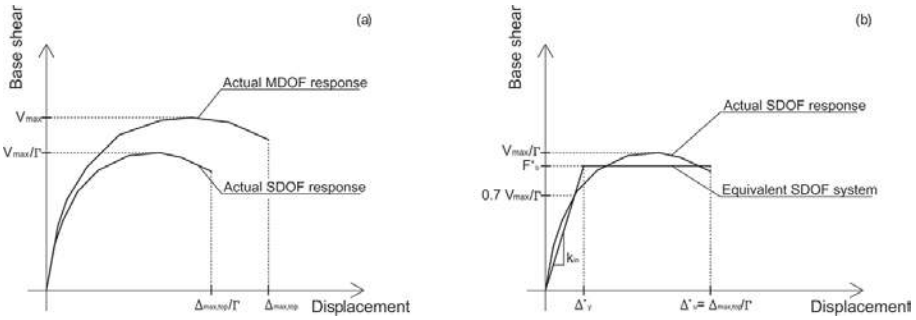

FIGURE 14 (a) Design acceleration spectrum adopted for the evaluation of the N2 method; (b-f) identification of the performance points in the acceleration-displacement response spectra diagram for the maximum PGA that the structures withstand.

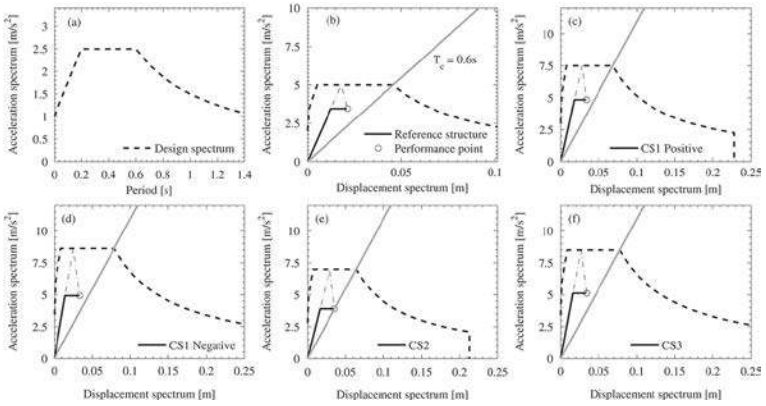

TABLE 1 Mechanical properties adopted for shell-model.

Materials	Material properties	Shell-model	Material test results
Bricks	E_{bx} [GPa]	5.60	9.80
	E_{by} [GPa]	5.60	4.70
	f_{tb} [MPa]	1.4	-
	G^I_b [N/mm]	0.08	-
Mortar joints	μ [-]	0.63	0.63
	c [MPa]	0.38	0.38
	f_{tm} [MPa]	0.30	$f_{tm} = c/(2\mu)$
	K_{nn} [MN/m^3]	3.00 x 10^5	-

	K_{tt} [MN/m^3]	1.00 x 10^4	-
	G^I_f [N/mm]	0.41	-
	G^{II}_f [N/mm]	0.50	-
Masonry walls	E_{mv} [GPa]	-	5.10
	E_{mh} [GPa]	-	1.28
Concrete	E_c [GPa]	34.5	34.5
	f_c & f_{cc} [MPa]	51.4 (unconfined) 80.0 (confined – RC walls) 75.0 (confined – RC beams)	51.4

	f_{tc} [MPa]	3.00	3.00
Reinforcing bars	f_y [MPa]	540	537
	f_u [MPa]	600	625

E_{bx}: brick E-modulus for loading along the brick's height;

E_{by}: brick E-modulus for loading along the brick's length;

f_{tb}: brick tensile strength;

G^I_b: brick fracture energy;

μ and c: interface friction and cohesion coefficient;

f_{tm}: interface tensile strength;

K_{nn} and K_{tt}: interface normal and tangent stiffness;

G^I_f and G^{II}_f: interface Mode I and II fracture energy;

E_{mv} and E_{mh}: vertical and horizontal masonry E-modulus;

E_c: concrete E-modulus;

f_c and f_{cc}: confined and unconfined concrete compressive strength;

f_y and f_u: reinforcing bar yield and ultimate tensile strength, [SIA162/1, 1995].

TABLE 2 Adopted material properties for macro-model.

Materials	Material properties	Macro-model	Material test results
URM members	μ^* / μ [-]	0.15 (TU1) 0.24 (TU2)	0.63
	c^* / c [MPa]	0.23 (TU1) 0.20 (TU2)	0.38
	f_m [MPa]	6.30	6.30
	E_{mv} [GPa]	5.10	5.10
	G_m [GPa]	0.54	-
	Gc_t [-]	1.00	-
	β [-]	0.00	-
RC members	E_c [GPa]	E_{eff} (1st storey & beams)	36.0

		18.0 (above storeys)	36.0
	G_c [GPa]	E_{eff}/2.4 (1st storey & beams)	7.50
		7.50 (above storeys)	7.50
	f_y [MPa]	550	537

μ^* and c^*: equivalent friction and cohesion coefficients;

μ and c: friction and cohesion coefficient from triplet tests;

f_m: masonry compressive strength;

E_{mv}: E- modulus of masonry panels subjected to compression orthogonal to bed-joints;

G_m: masonry shear modulus;

Gc_t: shear deformability parameter;

β: softening parameter;

E_c and G_c: RC member's Young's and shear modulus;

f_y: reinforcing bar yield tensile strength adopted in RC members.

TABLE 3 RC member's reinforcement ratios.

RC walls	ρ_{mean} (case studies 1 & 2)	0.26 %
	ρ_{mean}(case study 3)	0.35 %
RC beams	$\rho_{b,top} = \rho_{b,bot} = \rho_b$	0.90 %

ρ_{mean}: longitudinal reinforcement ratio in RC walls;

$\rho_{b,top} = \rho_{b,bot} = \rho_b$: top and bottom longitudinal reinforcement ratios (RC beams).

TABLE 4 Increase in drift capacity for the three case studies.

	Average drift capacity [%]	Increase in drift capacity [%]
Reference structure	0.24 %	-
Case study 1 - Pos.	0.36 %	+ 50 %
Case study 1 - Neg.	0.36 %	+ 50 %
Case study 2	0.38 %	+ 58 %
Case study 3	0.37 %	+ 54 %

TABLE 5 Definition of the bi-linear envelope of the equivalent SDOF.

Parameters for the bi-linear envelope	Proposed criteria
(i) Maximum shear F^*_b	F^*_b is determined so that the energy dissipated by the equivalent SDOF and the actual SDOF systems are equal (Fig. 13b)
(ii) Initial stiffness k_{in}	k_{in} is the secant stiffness at $0.70\ V_{max}/\Gamma$ (Fig. 13b)
(iii) Ultimate drift δ_u	δ_u corresponds to the displacement Δ^*_u divided the height of the structure

V_{max}: maximum shear force (actual MDOF response);

F^*_b: maximum shear force (equivalent SDOF system);

k_{in}: initial stiffness (equivalent SDOF system);

δ_u: ultimate average drift (equivalent SDOF system);

$\Delta^*_u = \Delta_{max,top} / \Gamma$: ultimate displacement (actual SDOF response);

$\Delta_{max,top}$: ultimate top displacement (actual MDOF response);

Γ: transformation factor calculated according to EN 1998-1 [2004].

TABLE 6 Comparison between the reference structure and the three case studies (except for the equivalent period T^* and $PGA_{max,abs}$ values of the reference structure taken as unit).

	Reference structure	Case study 1- Pos.	Case study 1- Neg.	Case study 2	Case study 3
T^*	0.38 s	0.38 s	0.34 s	0.41 s	0.35 s
$PGA_{max,abs}$	2.0 m/s^2	3.0 m/s^2	3.4 m/s^2	2.8 m/s^2	3.4 m/s^2
Δ^*_y	1.00	1.45	1.15	1.31	1.28
Δ^*_u	1.00	1.50	1.50	1.58	1.52
μ^*	1.00	1.04	1.30	1.21	1.19
F^*_b	1.00	1.42	1.45	1.50	2.02
PGA_{max}	1.00	1.50	1.70	1.38	1.68

T^*: equivalent period (equivalent SDOF system);

$PGA_{max,abs}$: absolute maximum PGA the structures can sustain;

Δ^*_y: normalised yield displacement (equivalent SDOF system);

Δ^*_u: normalised ultimate displacement (equivalent SDOF system);

μ^*: normalised system's displacement ductility (equivalent SDOF system);

F^*_b: normalised total base shear (equivalent SDOF system);

PGA_{max}: normalised maximum PGA the structures can sustain.